Draft version January 30, 2003
Preprint typeset using LaTeX style emulateapj v. 14/09/00

RADIO ASTRONOMICAL POLARIMETRY AND PHASE-COHERENT MATRIX CONVOLUTION

W. van Straten
Centre for Astrophysics and Supercomputing, Swinburne University of Technology,
Hawthorn, VIC 3122, Australia
wvanstra@pulsar.physics.swin.edu.au

Draft version January 30, 2003

ABSTRACT

A new phase-coherent technique for the calibration of polarimetric data is presented. Similar to the one-dimensional form of convolution, data are multiplied by the response function in the frequency domain. Therefore, the system response may be corrected with arbitrarily high spectral resolution, effectively treating the problem of bandwidth depolarization. As well, the original temporal resolution of the data is retained. The method is therefore particularly useful in the study of radio pulsars, where high time resolution and polarization purity are essential requirements of high-precision timing. As a demonstration of the technique, it is applied to full-polarization baseband recordings of the nearby millisecond pulsar, PSR J0437−4715.

Subject headings: methods: data analysis — pulsars: individual (PSR J0437-4715) — techniques: polarimetric

1. INTRODUCTION

In radio polarimetry, two orthogonal senses of polarization are received and propagated through separate signal paths. Each signal therefore experiences a different series of amplification, attenuation, mixing, and filtering before sampling or detection is performed. Whereas efforts are made to match the components of the observatory equipment, each will realistically have a unique frequency response to the input signal. Even a simple mismatch in signal path length will result in a relative phase difference between the two polarizations that varies linearly with frequency.

In fact, any physically realizable system will transform the radiation in a frequency-dependent manner. Where variations across the smallest bandwidth available may be considered negligible, post-detection calibration and correction techniques may be used to invert the transformation and recover the original polarimetric state. However, the transformation may vary significantly across the band, causing the polarization vector to combine destructively when integrated in frequency. This phenomenon is known as "bandwidth depolarization" of the signal, and results in irreversible decimation of the degree of polarization.

It is therefore desirable to perform polarimetric corrections at sufficiently high spectral resolution, which is available only at the cost of temporal resolution unless phase coherence is maintained. Conventional post-detection correction techniques therefore prove insufficient when high time resolution is also a necessity. For example, certain pulsar experiments require high time resolution in order to resolve key features in the average pulse profile. As well, it has been shown that insufficient time resolution can also lead to depolarization (Gangadhara *et al.* 1999). These considerations motivate the development of a method for phase-coherent polarimetric transformation. Further impetus is provided by the growing number of baseband recording systems at observatories around the world, the enhanced flexibility made available through use of off-line data reduction software, and the increasing computational power of affordable facilities.

A method has previously been presented for the phase-coherent correction of interstellar dispersion smearing. Convolution is performed by multiplying the spectrum of baseband data with the inverted frequency response of the interstellar medium (ISM), as modeled by the cold plasma dispersion relation (Hankins & Rickett 1975). The current development extends the concept of convolution to multiplication of the vector spectrum by the inverse of the frequency response matrix. The term "matrix convolution" is used to distinguish this operation from two-dimensional convolution, such as would be performed on an image. Whereas the frequency response matrix may be composed of various factors, such as those arising from the ISM and ionosphere, this paper will be restricted to considering only the instrumental response.

Following a brief review of matrix convolution and its relationship to the transformation properties of radiation, a technique is proposed by which the instrumental frequency response matrix may be determined and used to calibrate phase-coherent baseband data. As a preliminary illustration, the method is applied to full-polarization observations of the millisecond pulsar, PSR J0437−4715, from two different receiver systems. The results agree well with previously published polarimetry for this pulsar (Navarro *et al.* 1997).

2. MATRIX CONVOLUTION

Consider a linear system with impulse response, $j(t)$. Presented with an input signal, $e(t)$, the output of this system is given by the convolution, $e'(t) = j(t) * e(t)$. In the two-dimensional case, each output signal is given by a linear combination of the input signals,

$$e'_1(t) = j_{11}(t) * e_1(t) + j_{12}(t) * e_2(t), \quad (1)$$

$$e'_2(t) = j_{21}(t) * e_1(t) + j_{22}(t) * e_2(t). \quad (2)$$

Now let $e_1(t)$ and $e_2(t)$ be the complex-valued analytic signals associated with two real time series, providing the instantaneous amplitudes and phases of two orthogonal

senses of polarization. By defining the analytic vector, $\boldsymbol{e}(t)$, with elements $e_1(t)$ and $e_2(t)$, and the 2×2 impulse response matrix, $\mathbf{j}(t)$, with elements $j_{mn}(t)$, we may express the propagation of a transverse electromagnetic wave by the matrix equation,

$$\boldsymbol{e}'(t) = \mathbf{j}(t) * \boldsymbol{e}(t). \quad (3)$$

By the convolution theorem, equation (3) is equivalent to

$$\boldsymbol{E}'(\nu) = \mathbf{J}(\nu)\boldsymbol{E}(\nu), \quad (4)$$

where $\mathbf{J}(\nu)$ is the frequency response matrix with elements $J_{mn}(\nu)$, and $\boldsymbol{E}(\nu)$ is the vector spectrum. In the case of monochromatic light, or under the assumption that $\mathbf{J}(\nu)$ is constant over all frequencies, matrix convolution reduces to simple matrix multiplication in the time domain, as traditionally represented using the Jones matrix. However, because these conditions are not physically realizable, the Jones matrix finds its most meaningful interpretation in the frequency domain.

The average auto- and cross-power spectra are neatly summarized by the average power spectrum matrix, defined by the vector direct product, $\bar{\mathbf{P}}(\nu) = \langle \boldsymbol{E}(\nu) \otimes \boldsymbol{E}^\dagger(\nu) \rangle$, where $\boldsymbol{E}^\dagger$ is the Hermitian transpose of $\boldsymbol{E}$ and the angular brackets denote time averaging. More explicitly:

$$\bar{\mathbf{P}}(\nu) = \begin{pmatrix} \langle E_1(\nu) E_1^*(\nu) \rangle & \langle E_1(\nu) E_2^*(\nu) \rangle \\ \langle E_2(\nu) E_1^*(\nu) \rangle & \langle E_2(\nu) E_2^*(\nu) \rangle \end{pmatrix}. \quad (5)$$

Each component of the average power spectrum matrix, $\bar{P}_{mn}(\nu)$, is the Fourier transform pair of the average correlation function, $\bar{\rho}_{mn}(\tau)$ (Papoulis 1965). Therefore, $\bar{\mathbf{P}}(\nu)$ may be related to the commonly used coherency matrix,

$$\boldsymbol{\rho} = \langle \boldsymbol{E}(t) \otimes \boldsymbol{E}^\dagger(t) \rangle = \bar{\boldsymbol{\rho}}(0) = \frac{1}{2\pi} \int_{\nu_0 - \Delta\nu}^{\nu_0 + \Delta\nu} \bar{\mathbf{P}}(\nu) d\nu, \quad (6)$$

where ν_0 is the centre frequency and $2\Delta\nu$ is the bandwidth of the observation. The average power spectrum matrix may therefore be interpreted as the coherency spectral density matrix and, in the limit $\Delta\nu \to 0$, $\boldsymbol{\rho} = \bar{\mathbf{P}}(\nu_0)/2\pi$.

Using equations (4) and (5) it is easily shown that a two-dimensional linear system transforms the average power spectrum as

$$\bar{\mathbf{P}}'(\nu) = \mathbf{J}(\nu)\bar{\mathbf{P}}(\nu)\mathbf{J}^\dagger(\nu). \quad (7)$$

This matrix equation is called the congruence transformation, and forms the basis on which the frequency response of a system will be related to the input (source) and output (measured) coherency spectrum. For brevity in the remainder of this paper, all symbolic values are assumed to be a function of frequency, ν, unless explicitly stated otherwise.

3. ISOMORPHIC REPRESENTATIONS

The subject of radio astronomical polarimetry received its most rigorous and elegant treatment with the two separate developments of Britton (2000) and Hamaker (2000). Whereas Britton illuminates the isomorphism between the transformation properties of radiation and those of the Lorentz group, Hamaker illustrates and utilizes the similarity with the multiplicative quaternion group. The salient features of both formalisms provide a sound foundation for the current development, and merit a brief review.

Any complex 2×2 matrix, $\mathbf{J}$, may be expressed as

$$\mathbf{J} = J_0\mathbf{I} + \boldsymbol{J} \cdot \boldsymbol{\sigma}, \quad (8)$$

where J_0 and $\boldsymbol{J} = (J_1, J_2, J_3)$ are complex, $\mathbf{I}$ is the 2×2 identity matrix, and $\boldsymbol{\sigma}$ is a 3-vector whose components are the Pauli spin matrices. The 4-vector, $[J_0, \boldsymbol{J}]$, may be treated using the same algebraic rules as those used for quaternions. In the remainder of this paper, the equivalent quaternion and 2×2 matrix forms (as related by eq. [8]) will be interchanged freely.

If $\mathbf{J}$ is Hermitian, then the components of $[J_0, \boldsymbol{J}]$ are real. The average power spectrum and coherency matrices are Hermitian and, when decomposed in this manner, $2[S_0, \boldsymbol{S}]$ may be interpreted as the mean Stokes parameters, where $2S_0$ is the total intensity and $2\boldsymbol{S}$ is the polarization vector. By writing $\bar{\mathbf{P}} = [\bar{S}_0, \bar{\boldsymbol{S}}]$, it is more easily seen that the integration of equation (6) leads to bandwidth depolarization when the orientation of $\bar{\boldsymbol{S}}$ varies with ν.

An arbitrary 2×2 matrix may also be represented by the polar decomposition,

$$\mathbf{J} = J\, \mathbf{B}_{\hat{\boldsymbol{m}}}(\beta)\mathbf{R}_{\hat{\boldsymbol{n}}}(\phi), \quad (9)$$

where $J = (\det \mathbf{J})^{1/2}$,

$$\mathbf{B}_{\hat{\boldsymbol{m}}}(\beta) = \exp(\boldsymbol{\sigma}\cdot\hat{\boldsymbol{m}}\beta) = [\cosh\beta, \sinh\beta\ \hat{\boldsymbol{m}}], \quad (10)$$

$$\mathbf{R}_{\hat{\boldsymbol{n}}}(\phi) = \exp(i\,\boldsymbol{\sigma}\cdot\ \hat{\mathbf{n}}\phi) = [\cos\phi, i\sin\phi\ \hat{\mathbf{n}}], \quad (11)$$

and $\hat{\boldsymbol{m}}$ and $\hat{\mathbf{n}}$ are real-valued unit 3-vectors. The matrix, $\mathbf{R}_{\hat{\boldsymbol{n}}}(\phi)$, is unitary and, beginning with equation (7), it can be shown to preserve the degree of polarization and rotate $\boldsymbol{S}$ about the axis, $\hat{\mathbf{n}}$, by an angle 2ϕ. Similarly, the Hermitian matrix, $\mathbf{B}_{\hat{\boldsymbol{m}}}(\beta)$, can be shown to perform a Lorentz boost on the 4-vector, $[S_0,\ \boldsymbol{S}]$, along the axis, $\hat{\boldsymbol{m}}$, by a velocity parameter 2β (Britton 2000).

As both $\mathbf{B}_{\hat{\boldsymbol{m}}}(\beta)$ and $\mathbf{R}_{\hat{\boldsymbol{n}}}(\phi)$ are unimodular, the congruence transformation (eq. [7]) preserves the determinant up to a multiplicative constant, $|J|^2$, ie. $\det \bar{\mathbf{P}}' = |J|^2 \det \bar{\mathbf{P}}$. Britton notes that $\det \bar{\mathbf{P}} = \bar{S}_0^2 - |\bar{\boldsymbol{S}}|^2 = \bar{S}_{\rm inv}^2$ is simply the Lorentz invariant, which he calls the polarimetric invariant interval. He also proposes that a mean pulsar profile formed using the invariant interval may be used for high-precision pulsar timing. Whereas the boost component of the system response distorts the total intensity profile in a time-dependent manner, the invariant interval remains stable, providing a superior basis for arrival time estimates and a robust alternative to polarimetric calibration. However, the invariant interval is not preserved in the presence of bandwidth depolarization, further motivating the current development.

4. DETERMINATION OF THE SYSTEM RESPONSE

In principle, any method by which the frequency response matrix may be derived with sufficiently high resolution could be adapted for use with the matrix convolution approach. A number of different parameterizations and techniques have previously been presented for the calibration of single-dish radio astronomical instrumental polarization (Stinebring *et al.* 1984; Turlo *et al.* 1985; Xilouris 1991; Britton 2000). The current treatment follows the parameterization chosen by Hamaker (2000), including polar decomposition of the system response followed by application of the congruence transformation. This approach offers a number of significant advantages. For instance, in the derivation of the solution, it is unnecessary to make any small-angle approximations and, when compared to the manipulations of 4×4 Mueller matrices,

the equivalent quaternion and 2×2 Jones matrix representations greatly simplify the required algebra. As well, equations (7) and (9) are specific to no particular basis, permitting the application of the formalism to a variety of feed designs by proper choice of the basis matrices, $\boldsymbol{\sigma}$. Perhaps most importantly, as shown by Hamaker and discussed below, the polar decomposition enables the determination of the boost component of the system response using only an observation of an unpolarized source. This simplification has beneficial impact on experiments where only the total intensity or fractional degree of polarization are of concern.

Consider the reception of unpolarized radiation, which has an input average power spectrum matrix, $\bar{\mathbf{P}}_L = \mathbf{I}\ T_0/2$, where $\mathbf{I}$ is the identity matrix and T_0 is the total intensity. Beginning with equations (7) and (9), the output average power spectrum can be trivially shown to be

$$\bar{\mathbf{P}}'_L = \mathbf{B}_{\hat{\boldsymbol{m}}}(\beta)^2\ |J|^2 T_0/2. \tag{12}$$

Notice that the phase of J is lost in the detection of the average power spectrum. For this reason, the current technique is insensitive to absolute phase terms arising in the frequency response of the system, and may be used to determine only the relative phase differences between its components. The scalar factors, $|J|^2$ and T_0, are easily determined in a separate flux calibration procedure that will not be considered presently. Therefore, $\mathbf{B}_{\hat{\boldsymbol{m}}}(\beta)$ may be found by taking the positive Hermitian square root of the measured average power spectrum matrix of an unpolarized source (see Appendix A).

This simple result merits closer inspection. The system response may be corrected by inverting equation (4), that is, by calculating $\boldsymbol{E} = \mathbf{J}^{-1}\boldsymbol{E'}$. Notice that, under the polar decomposition chosen in equation (9), the boost transformation is the first to be inverted. That is, regardless of the unknown rotation, the boost solution may be used to completely invert the distortion of total intensity, S_0. This consequence of the polar decomposition has considerable impact in the field of high-precision pulsar timing, where the average total intensity profile is used to determine the pulse time of arrival. Polarimetric distortions to the total intensity can significantly alter the shape of this profile and systematically alter arrival time estimates, especially as a function of parallactic angle, or with fluctuations of ionospheric total electron content. With the boost component thus determined, the resulting distortions to total intensity can, in principle, be completely corrected.

It remains to solve for the rotation component of $\mathbf{J}$, which may be determined using observations of calibrators with known polarization. Given the known boost, $\mathbf{B}_{\hat{\boldsymbol{m}}}(\beta)$, input polarization state, $\bar{\mathbf{P}}_n$, and measured output state, $\bar{\mathbf{P}}'_n$, equation (7) is solved for the rotation, $\mathbf{R}_{\hat{\boldsymbol{n}}}(\phi)$. Considering the equivalent three-dimensional Euclidian rotation, $\mathbf{R}_{\hat{\boldsymbol{n}}}{}^{(3)}(2\phi)$, of the polarization vector, $\boldsymbol{S}$, it is easily seen that, given a single pair of input, $\boldsymbol{S_1}$, and output, $\boldsymbol{S_1}'$, polarization vectors, the rotations that solve $\boldsymbol{S_1}' = \mathbf{R}_{\hat{\boldsymbol{n}}}{}^{(3)}(2\phi)\boldsymbol{S_1}$, where $|\boldsymbol{S_1}'| = |\boldsymbol{S_1}|$, form an infinite set of rotations with axis confined only to a plane. Therefore, an observation of a second, non-collinear calibrator source is required in order to uniquely determine the system response rotation.

Many receivers are equipped with a linearly polarized noise diode that may be used to inject a calibrator signal into the feed horn. This noise diode may be switched using a wide-band, amplitude-modulated square-wave. The "off" or "low" fraction of the wave consists of only the system plus sky temperature, which shall be assumed to be unpolarized. The "on" or "high" fraction of the wave contains additional linearly polarized radiation, described in quaternion form by

$$\bar{\mathbf{P}}_H = [1, (\cos 2\Psi, \sin 2\Psi, 0)]\ C_0/2, \tag{13}$$

where C_0 is the flux and Ψ is the position angle of the calibrator diode. A single linear noise diode provides only one known input calibrator state. Unless another calibrator is available, the technique must be modified to solve for a reduced representation of the system response. For the calibration described in this paper, $\mathbf{R}_{\hat{\boldsymbol{n}}}(\phi)$ was be decomposed into two rotations: $\mathbf{R}_{\hat{\boldsymbol{v}}}(\Delta\Psi)$, allowing imperfect alignment of the noise diode; followed by $\mathbf{R}_{\hat{\boldsymbol{q}}}(\Phi_I)$, allowing a differential path length between the two linear polarizations (see Appendix A). It is important to distinguish $\Delta\Psi$ and Φ_I from the actual parameters of the receiver, as the polar decomposition does not model the order in which the transformations physically occur.

4.1. *Calibrator Observations*

When observing the artificial calibrator, it is important that the noise diode be switched on a time-scale much shorter than the interval over which the digitization thresholds are reset, in order that $\bar{\mathbf{P}}_H$ may be differentiated from the baseline, $\bar{\mathbf{P}}_L$. However, the calibrator period must also be long enough to provide distinct on-pulse and off-pulse time samples in the synthesized filterbank. Given the sampling interval, t_s, of the baseband recorder, the calibrator period, T_C, should be at least $T_C \geq n_b t_s N$, where N is the number of channels in the synthetic filterbank and n_b is the desired number of phase bins in the integrated calibrator profile. In order to achieve clear separation of on-pulse and off-pulse states, $n_b = 64$ was chosen. As well, it was found that a filterbank with $N = 2048$ channels sufficiently resolved the features of the frequency response.

For each hour-long observation of PSR J0437−4715, the pulsed calibrator was recorded for 4.5 minutes, ensuring sufficient signal-to-noise in each channel of the synthetic filterbank. Data were reduced offline using `psrdisp`, a software package developed to process pulsar baseband data, described in the following section. After forming a synthetic filterbank, the Stokes parameters in each channel were detected and folded at the pulsed calibrator period. High and low state polarimetric passbands were formed from the average on- and off-pulse Stokes parameters of the calibrator profile in each channel. These passbands were median filtered to remove spurious radio-frequency interference, and interpolated to the required frequency resolution, as dictated by the parameters of the coherent dedispersion kernel. From this high frequency-resolution polarimetric representation of the calibrator, the frequency response matrix was computed as described in Appendix A. Figure 1 plots representative examples of the determined frequency response parameters at 660 MHz and 1247 MHz. The inverse of the frequency response matrix was used in the convolution kernel when reducing the pulsar observations, as described in the next section.

5. PULSAR OBSERVATIONS

Dual-polarization baseband data from the nearby millisecond pulsar, PSR J0437−4715, were recorded during 2001 June 26-28, using the 64 m dish at the Parkes Observatory. As a test of phase-coherent calibration in the pathological case (refer to Figure 2), the 50 cm receiver was used to record 3.6 hours of data at 660 MHz. As well, a total of 7 hours was recorded at 1247 MHz, using the centre element of the Multibeam receiver. The radio and intermediate frequency signals were quadrature downconverted, band-limited to 20 MHz, two-bit sampled, and recorded using the Caltech-Parkes-Swinburne Recorder (CPSR) (van Straten, Britton, & Bailes 2000). The digitized data were processed offline at Swinburne University's supercomputing facilities using `psrdisp`, a flexible software package that implements a number of baseband data reduction options.

The four channels of two-bit quantized data were corrected using the dynamic level-setting technique (Jenet & Anderson 1998) and combined to form the digitized analytic vector, $\boldsymbol{e}(t_i)$. This vector was convolved while synthesizing a 16-channel coherent filterbank (Jenet *et al.* 1997), a process described in more detail in Appendix B. In each channel, the Stokes 4-vector, $[S_0, \boldsymbol{S}](\nu_k, t_n)$, was detected and integrated as a function of pulse phase, given by t_n modulo the predicted topocentric period. Pulse period and absolute phase were calculated using a polynomial generated by the `tempo` software package (http://pulsar.princeton.edu/tempo).

Each 1 GB segment of baseband data (representing approximately 53.7 seconds) was processed in this manner, producing average pulse profiles with 4096 phase bins, or a resultant time resolution of approximately 1.4 μs. Each archive was later corrected for parallactic angle rotation of the receiver feeds before further integrating in time to produce hour-long average profiles. These were flux calibrated using observations of Hydra A, which was assumed to have a flux density of approximately 85 Jy at 660 MHz and 48 Jy at 1247 MHz. The flux calibrated archives were then integrated in time and frequency, producing the mean pulse profiles presented in Figure 3. In these plots, the linearly polarized component, L, is given by $L^2 = Q^2 + U^2$ and the position angle, ψ, where $\tan\psi = U/Q$, has been plotted twice, at $\psi \pm \pi/2$. Comparison with the uncalibrated profiles in Figure 4 indicates significant restoration of the polarized component at both frequencies. As well, the calibrated average profiles agree satisfactorily with previously published polarization data for PSR J0437−4715 (Navarro *et al.* 1997).

6. DISCUSSION

Prior to its reception, the radiation from a pulsar must propagate through the magnetized plasma of the ISM, resulting in Faraday rotation of the position angle, ψ. The change in position angle is given by $\Delta\psi = RM\lambda^2$, where RM is the rotation measure and λ is the wavelength. Therefore, one motivation for a pulsar polarimetry experiment is the determination of the RM along the line of sight to the pulsar. Combined with a dispersion measure estimate, the RM can provide information about the galactic magnetic field strength and direction. When the RM is very small, as it is for PSR J0437−4715, $\Delta\psi$ is not detectable across a single 20 MHz bandpass. Therefore, two observations widely separated in frequency are required in order to obtain an estimate. However, as there exists an unknown feed offset between 50 cm and Multibeam receivers that remains uncalibrated in the current treatment, no estimation of rotation measure is presently offered.

For pulsars with known RM, matrix convolution enables phase-coherent Faraday rotation correction by addition of $\Delta\psi$ to $\Delta\Psi$ in equation (A1). This approach would further treat the problem of bandwidth depolarization, especially for sources with large rotation measures observed at lower frequencies.

As phase-coherent calibration corrects the undetected voltages, any measurements derived from these data will also be implicitly calibrated. This includes not only the coherency products but also other statistical values such as the higher order moments, modulation index, and polarization covariance. The method may therefore find application in experiments which aim to describe pulse shape fluctuations (Jenet, Anderson, & Prince 2001) or variations of the galactic magnetic field along the line of sight (Melrose & Macquart 1998), for example.

Although matrix convolution may in principle be used to completely correct baseband data, a full solution of the system response is lacking in the current treatment. Perhaps a technique may be developed which combines the use of pulsars (Stinebring *et al.* 1984; Xilouris 1991) with high-resolution determination of the frequency response matrix. This approach would include tracking a bright, strongly polarized pulsar over a wide range of parallactic angles, followed by fitting a model of the instrumental response to the measured Stokes parameters. As it is nontrivial to model the effects of phenomena that may change over the course of such a calibration, such as fluctuations in ionospheric total electron content, it may prove more feasible to install a second artificial noise diode in the receiver feed horn. Oriented with a position angle offset from the first by approximately 45°, it would provide a more readily available and reliable means of regularly solving for $\mathbf{R}_{\hat{\boldsymbol{n}}}(\phi)$. Alternatively, a single noise diode could be mechanically rotated with respect to the feeds, obviating the inevitable cross-talk that would arise between two diodes. Consideration of these options may benefit future feed horn design.

The observations of PSR J0437−4715 presented in the previous section serve to illustrate the strength the matrix convolution technique, highlighting its ability to recover data which has been severely corrupted by the observatory instrumentation. Perhaps the most rigorous test of the methodology will be derived from the unsurpassed timing accuracy of PSR J0437−4715 (van Straten *et al.* 2001). Calibration errors translate into systematic timing errors, and any deficiency in the characterization of the system response would manifest itself in the arrival time residuals of this remarkable pulsar.

The Parkes Observatory is part of the Australia Telescope which is funded by the Commonwealth of Australia for operation as a National Facility managed by CSIRO. This research was supported by the Commonwealth Scholarship and Fellowship Plan. I am grateful to Matthew Britton and Simon Johnston, with whom I have shared many stimulating discussions on radio polarimetry. Thanks also to Matthew Bailes and Stephen Ord for assistance with observing and helpful comments on the text.

APPENDIX

SOLUTION OF SYSTEM RESPONSE

The instrumental frequency response matrix used in calibrating the data presented in this paper was parameterized by

$$\mathbf{J} = \mathbf{B}_{\hat{\boldsymbol{m}}}(\beta)\mathbf{R}_{\hat{\boldsymbol{q}}}(\Phi_I)\mathbf{R}_{\hat{\boldsymbol{v}}}(\Delta\Psi). \tag{A1}$$

The boost component may be solved most easily using the quaternion form of equation (12),

$$[\bar{L}'_0, \bar{\boldsymbol{L}}'] = \exp(2\,\boldsymbol{\sigma}\cdot\,\hat{\boldsymbol{m}}\beta)|J|^2T_0 = [\cosh(2\beta), \sinh(2\beta)\hat{\boldsymbol{m}}]\;|J|^2T_0, \tag{A2}$$

where $[\bar{L}'_0, \bar{\boldsymbol{L}}']$ are the measured off-pulse Stokes parameters, producing

$$\beta = \frac{1}{2}\tanh^{-1}\left(\frac{|\bar{\boldsymbol{L}}'|}{\bar{L}'_0}\right) \qquad \text{and} \qquad \hat{\boldsymbol{m}} = \frac{\bar{\boldsymbol{L}}'}{|\bar{\boldsymbol{L}}'|}. \tag{A3}$$

The two rotations, $\mathbf{R}_{\hat{\boldsymbol{q}}}(\Phi_I)$ and $\mathbf{R}_{\hat{\boldsymbol{v}}}(\Delta\Psi)$, may be determined by considering the equivalent three-dimensional Euclidian rotations, $\mathbf{R}_{\hat{\boldsymbol{q}}}{}^{(3)}(2\Phi_I)$ and $\mathbf{R}_{\hat{\boldsymbol{v}}}{}^{(3)}(2\Delta\Psi)$, of the input polarization vector. Given that the noise diodes installed in the receivers at the Parkes radio-telescope have a position angle nearly equal to 45°, the input Stokes parameters are $[1, \bar{\boldsymbol{H}}]C_0$, where $\bar{\boldsymbol{H}} = (0, 1, 0)$ (cf. eq. [13]). Therefore, Φ_I and $\Delta\Psi$ may be found by solving

$$\bar{\boldsymbol{H}}'' = \mathbf{R}_{\hat{\boldsymbol{q}}}{}^{(3)}(2\Phi_I)\mathbf{R}_{\hat{\boldsymbol{v}}}{}^{(3)}(2\Delta\Psi)\bar{\boldsymbol{H}}, \tag{A4}$$

where $\bar{\boldsymbol{H}}''$ is the normalized polarization vector after the observed Stokes parameters have been corrected for the boost. It is given by

$$[\bar{H}_0, \bar{\boldsymbol{H}}]'' = \mathbf{B}_{\hat{\boldsymbol{m}}}(\beta)^\dagger\bar{\mathbf{P}}'_H\mathbf{B}_{\hat{\boldsymbol{m}}}(\beta)/(|J|^2C_0), \tag{A5}$$

where $\bar{\mathbf{P}}'_H$ are the observed Stokes parameters. From equation (A4),

$$\Phi_I = \frac{1}{2}\tan^{-1}\left(\frac{-H''_3}{H''_2}\right) \qquad \text{and} \qquad \Delta\Psi = \frac{1}{2}\tan^{-1}\left(\frac{H''_1}{H''_2/\cos(2\Phi_I)}\right). \tag{A6}$$

Notice that $|J|^2$, T_0, and C_0 cancel out in each of equations (A3) and (A6), obviating the need to solve for these parameters at this stage. The vector components of the boost quaternion, $(B_1, B_2, B_3) = \sinh\beta\,\hat{\boldsymbol{m}}$, as well as Φ_I and $\Delta\Psi$, are plotted as a function of frequency in Figure 1.

PERFORMING MATRIX CONVOLUTION

It is assumed that the reader has some familiarity with the more common, one-dimensional form of cyclical convolution as it is performed in the frequency domain using the Fast Fourier Transform (FFT) (Press *et al.* 1992, §13.1). In the two-dimensional vector case, there are simply two unique processes sampled at the same time interval, say $p(t_i)$ and $q(t_i)$. A one-dimensional, N-point, forward FFT is performed separately on each of p and q, forming two spectra, $P(\nu_k)$ and $Q(\nu_k)$, $0 \le k < N$. Corresponding elements from each of the spectra are treated as the components of a column 2-vector, $\boldsymbol{E}(\nu_k) = (P(\nu_k), Q(\nu_k))$, and multiplied by the inverse of the frequency response matrix, forming $\boldsymbol{E}'(\nu_k) = \mathbf{J}^{-1}(\nu_k)\boldsymbol{E}(\nu_k)$ (cf. eq. [4]). The components of the result, $P'(\nu_k)$ and $Q'(\nu_k)$, are once again treated as unique spectra, and separately transformed back into the time domain using the one-dimensional backward FFT.

In the case of the pulsar data presented in this paper, $p(t_i)$ and $q(t_i)$ are the signals from the two linear feeds in the receiver, and $\mathbf{J}(\nu_k)$ consists of the instrumental frequency response matrix, as determined in Appendix A, multiplied by the dispersion kernel, $H(\nu_k)$ (Hankins & Rickett 1975). When synthesizing an M-channel coherent filterbank, $H(\nu_k)$ is divided in frequency into M distinct dispersion kernels, each tuned to the centre frequency of the resulting filterbank channel.

REFERENCES

Britton, M. C. 2000, ApJ, 532, 1240
Gangadhara, R. T., Xilouris, K. M., von Hoensbroech, A., Kramer, M., Jessner, A., & Wielebinski, R. 1999, A&A, 342, 474
Hamaker, J. P. 2000, A&AS, 143, 515
Hankins, T. H., & Rickett, B. J. 1975, in Methods in Computational Physics 14, Radio Astronomy (New York: Academic Press), 55
Jenet, F. A., & Anderson, S. B. 1998, PASP, 110, 1467
Jenet, F. A., Anderson, S. B., & Prince, T. A. 2001, ApJ, 546, 394
Jenet, F. A., Cook, W. R., Prince, T. A., & Unwin, S. C. 1997, PASP, 109, 707
Melrose, D., & Macquart, J. 1998, ApJ, 505, 921
Navarro, J., Manchester, R. N., Sandhu, J. S., Kulkarni, S. R., & Bailes, M. 1997, ApJ, 486, 1019
Papoulis, A. 1965, Probability, Random Variables, and Stochastic Processes (Sydney: McGraw-Hill)
Press, W. H., Teukolsky, S. A., Vetterling, W. T., & Flannery, B. P. 1992, Numerical Recipes: The Art of Scientific Computing (2^{nd} ed.; Cambridge: Cambridge University Press)
Stinebring, D. R., Cordes, J. M., Rankin, J. M., Weisberg, J. M., & Boriakoff, V. 1984, ApJS, 55, 247
Turlo, Z., Forkert, T., Sieber, W., & Wilson, W. 1985, A&A, 142, 181
van Straten, W., Britton, M., & Bailes, M. 2000, in ASP Conf. Ser. 202, Pulsar Astronomy - 2000 and Beyond, ed. M. Kramer, N. Wex, & R. Wielebinski (San Francisco: ASP), 283
van Straten, W., Bailes, M., Britton, M., Kulkarni, S. R., Anderson, S. B., Manchester, R. N., & Sarkissian, J. 2001, Nature, 412, 158, astro-ph/0108254
Xilouris, K. M. 1991, A&A, 248, 323

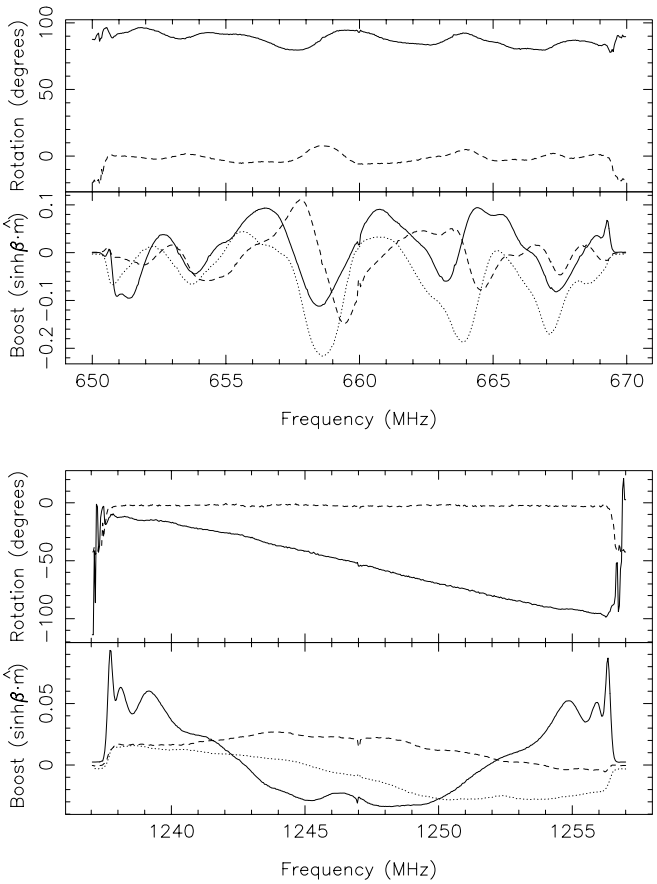

FIG. 1.— Frequency response at 50 cm (top) and 20 cm (bottom). For each band, the upper panel plots the rotation angles, $\Delta\Psi$ (dashed line) and Φ_I (solid line), and the lower panel plots the boost components along $\hat{\boldsymbol{q}}$ (solid line), $\hat{\boldsymbol{u}}$ (dotted line), and $\hat{\boldsymbol{v}}$ (dashed line). A signal path length mismatch between the two polarizations from the Multibeam (20 cm) receiver results in a linear differential phase (Φ_I) gradient across the bandpass.

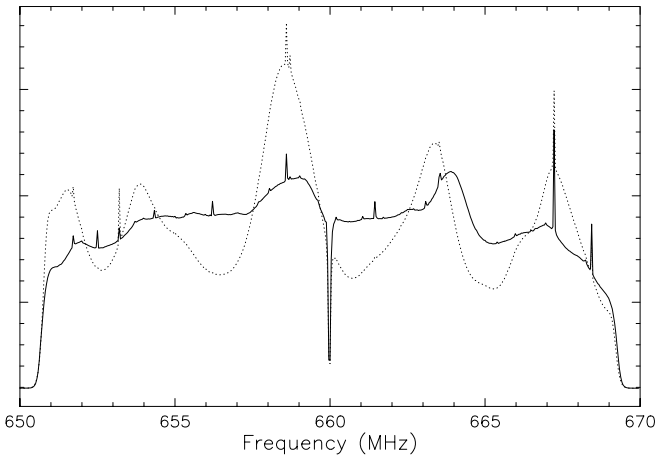

FIG. 2.— Average passbands from the two linear polarizations at 660 MHz. The gain in E_y (dotted line) varies wildly with frequency, evidencing the less than ideal condition of the 50 cm receiver.

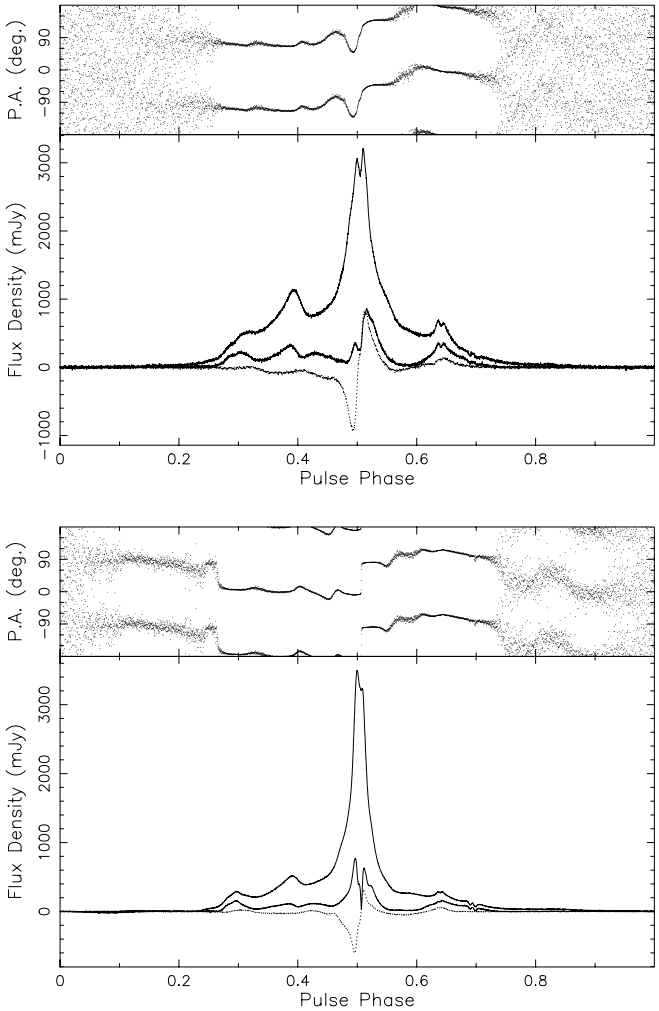

FIG. 3.— Average polarimetric pulse profiles of PSR J0437−4715 at 660 MHz (top) and 1247 MHz (bottom). The bottom panel of each plot displays the total intensity, Stokes I (upper solid line), the linearly polarized component, L (lower solid line), and the circularly polarized component, Stokes V (dotted line). The position angle, ψ, in the upper panel of each plot is shown without respect to any absolute frame of reference.

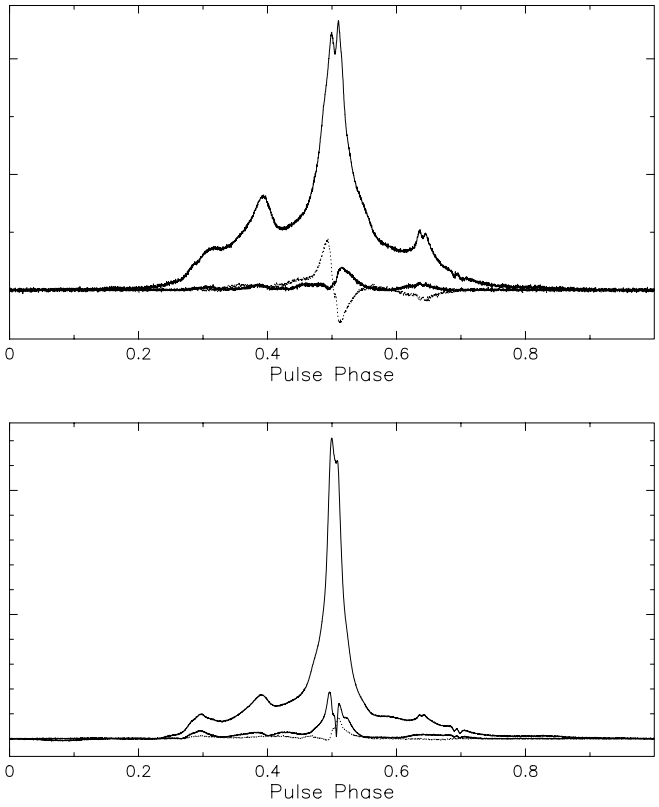

FIG. 4.— Uncalibrated average polarimetric pulse profiles of PSR J0437−4715 at 660 MHz (top) and 1247 MHz (bottom). Severe differential gain variation in the 50 cm bandpass (see Figure 2) has decimated the linearly polarized component at 660 MHz (top plot, lower solid line), whereas the differential phase gradient across the 20 cm bandpass (see Figure 1) has nearly eliminated the circularly polarized component at 1247 MHz (bottom plot, dotted line).